Catalysis Science & Technology

PAPER

View Article Online
View Journal | View Issue

Cite this: *Catal. Sci. Technol.*, 2015, 5, 2973

Post-synthesis incorporation of Al into germanosilicate ITH zeolites: the influence of treatment conditions on the acidic properties and catalytic behavior in tetrahydropyranylation

Mariya V. Shamzhy,[ab] Maksym V. Opanasenko,[ab] Francisca S. de O. Ramos,[ac] Libor Brabec,[a] Michal Horáček,[a] Marta Navarro-Rojas,[d] Russell E. Morris,[d] Heloise de O. Pastore[c] and Jiří Čejka*[a]

Received 3rd December 2014,
Accepted 12th March 2015

DOI: 10.1039/c4cy01594k

www.rsc.org/catalysis

Post-synthesis alumination of germanosilicate medium-pore ITH zeolites was shown to be an effective procedure for tuning their acidity. Treatment of ITH zeolites synthesized with different chemical compositions (*i.e.* Si/Ge = 2.5, 4.4 and 5.8) with aqueous $Al(NO_3)_3$ solution led to the formation of strong Brønsted and Lewis acid sites and an increasing fraction of ultramicro- and meso-pores in Ge-rich ITH samples (Si/Ge = 2.5 and 4.4). The concentration of Al incorporated into the framework increases with decreasing Si/Ge ratio of the parent ITH. The increasing temperature of alumination from 80 to 175 °C (HT conditions) resulted in (1) a 1.5–2-fold increase in the concentration of Brønsted acid sites formed and (2) a decreasing fraction of framework Al atoms detectable with base probe molecules (*i.e.* pyridine, 2,6-di-*tert*-butylpyridine), *i.e.* an increased concentration of the "inner" acid sites. The activity of prepared Al-substituted ITH zeolites in tetrahydropyranylation of alcohols is enhanced with increasing amount of accessible acid sites in bulky crystals (*e.g.* alumination at lower temperature) or with increasing total concentration of acid centres within tiny ITH crystals (*e.g.* alumination under HT conditions). This trend became more prominent with increasing kinetic diameter of the substrate molecules under investigation (methanol < 1-propanol < 1-hexanol).

1. Introduction

The role of zeolites in the current petroleum industry can hardly be overestimated. Aluminosilicate zeolites possessing strong acid centres have been widely used as heterogeneous catalysts for a great variety of processes.[1] The application of medium-pore zeolites as industrial catalysts and the recognition of the '*shape selective*' properties of these materials[2] have stimulated synthetic work aimed at preparing new microporous materials with various pore sizes and structures.[3–8]

Zeolite ITH, possessing three sets of interconnecting medium-pore 9- (4.0 × 4.9 Å), 10- (4.8 × 5.7 Å) and 10- (4.7 × 5.1 Å) ring channels, was first synthesized as a pure silicate in concentrated reaction mixtures ($H_2O/T^{IV} < 10$, where T is the zeolite framework tetrahedral atom) using hexamethonium as the structure-directing agent (SDA).[9] Introducing Al during the synthesis was reported to diminish the crystallization rate of ITH while favouring the formation of an EU-1 phase.[10] On the other hand, the smaller B–O–Si angles were claimed to facilitate the introduction of B into the ITH framework with respect to the EU-1 structure, although in relatively small amounts (Si/B ratios of >50).[10] Similarly, Al present in the initial gel was also reported to limit the crystallization field of germanosilicate UTL zeolites in favour of an STF phase,[11] while B influences the selectivity of UTL zeolite formation to a lesser extent.[12] Attempts to generate strong acid centres by post-synthesis alumination of borosilicate ITH zeolites resulted in an exchange of only a fraction of boron atoms yielding ITH with a Si/Al molar ratio of 80 (45 and 105 μmol g^{-1} of Brønsted and Lewis acid sites, respectively).[13] At the same time, Al-containing ITH zeolites with an increased concentration of Brønsted acid sites (63 and 48 μmol g^{-1} of

[a] *J. Heyrovský Institute of Physical Chemistry of the Czech Academy of Sciences, v. v. i., Dolejškova 3, CZ-182 23 Prague 8, Czech Republic. E-mail: jiri.cejka@jh-inst.cas.cz; Fax: +420 286 582 307; Tel: +420 266053795*
[b] *L. V. Pisarzhevskiy Institute of Physical Chemistry, National Academy of Sciences of Ukraine, pr. Nauki, 31 Kiev 03028, Ukraine; Fax: +380 445 256 216; Tel: +380 445 254 196*
[c] *Micro and Mesoporous Molecular Sieves Group, Institute of Chemistry, University of Campinas, Rua Monteiro Lobato, 270, 13083-861, Cidade Universitária Zeferino Vaz, Campinas, SP, Brazil*
[d] *EaStCHEM School of Chemistry, University of St. Andrews, St. Andrews KY16 9ST, United Kingdom*

Brønsted and Lewis acid sites, respectively) were synthesized directly only in the presence of Ge, exploiting its propensity to increase the nucleation rate of zeolites containing D4R SBUs (*e.g.*, **ITH**).[13] Al-**ITH** was shown to be a shape selective catalyst for conversion of aromatics[14] and catalytic cracking of vacuum gas oil producing propylene.[13]

Pure germanosilicate **ITH** zeolites characterized by Si/Ge ratios in the range 6–∞ were prepared using hexamethonium as a SDA.[15] Ge was found to preferentially occupy T-sites in the D4Rs.[15] Recently, Ren *et al.* reported the synthesis of Ge-enriched **ITH** zeolites ($2 < Si/Ge < 6$) in dilute medium (H_2O/T^{IV} = 22–66) using *N*,*N*,*N*′,*N*′-tetramethyl-1,6-hexanediamine (TMHDA) as the template.[16]

The possibility of tuning the strength of acid centres by post-synthesis substitution of B and Ge in the framework of borogermanosilicate large-pore **IWR** zeolites with Al and Ga was shown and confirmed by means of X-ray powder diffraction, chemical analysis and infrared spectroscopy of adsorbed pyridine.[17] The catalytic performance of prepared isomorphously substituted **IWR** zeolites in Friedel–Crafts acylation was also evaluated.[17]

In this paper, we successfully extended this approach to generate strong acid centres by post-synthesis alumination of medium-pore germanosilicate **ITH** zeolites. The formation of ultramicropores and mesopores at the expense of Ge extraction was observed when Ge-rich **ITH** zeolites with Si/Ge = 2.5 or 4.4 as starting materials were used. It was shown that the temperature of post-synthesis treatment strongly influenced the concentration of Brønsted acid sites formed and their accessibility. The improved catalytic behaviour of the aluminated **ITH** zeolites containing strong acid centres with respect to the initial germanosilicates was demonstrated in a tetrahydropyranylation reaction (Scheme 1) commonly used for protection of hydroxyl groups in peptide, nucleotide, carbohydrate, and steroid chemistry.[18]

2. Experimental part

2.1 Materials

1,6-Dibromohexane (96%), trimethylamine solution (31–35 wt.% in ethanol), *N*,*N*,*N*′,*N*′-tetramethyl-1,6-hexanediamine (99%), germanium oxide (99.99%), tetraethylorthosilicate (TEOS, 98%), and aluminium nitrate nonahydrate (≥98.5%) were used for synthesis and post-synthesis treatment of zeolites. 3,4-Dihydro-2*H*-pyran (DHP, 97%), methanol (≥99.9%), 1-propanol (≥99.9%), 1-hexanol (≥99.5%), mesitylene (≥99%) and hexane (≥97%) were used for catalytic experiments. All reactants and solvents were obtained from Sigma Aldrich and used as-received without any further treatment.

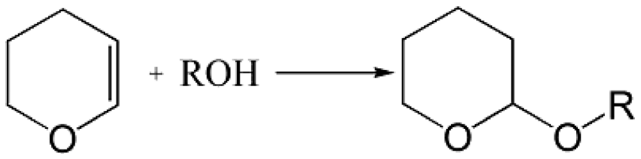

Scheme 1 Tetrahydropyranylation of alcohols.

2.2 Preparation of hexamethonium dihydroxide

Hexamethylenebis(trimethylammonium) dibromide was prepared according to ref. 19 and was transformed into the hydroxide form using a Bio-Rad AG-1X8 anion exchange resin. The solution of hexamethonium dihydroxide was concentrated (evaporated at p = 25 Torr, T = 35 °C) until the hydroxide concentration became 1.0 mol L^{-1}.

2.3 Synthesis of ITH zeolites

The zeolites prepared in this study were designated as *ITH-n*, where *n* is the Si/Ge ratio in the reaction mixture.

Ge-poor zeolite *ITH-6* was synthesized according to ref. 10 using hexamethonium dihydroxide as the SDA. The starting gel had the following composition: 0.86 (SiO_2) : 0.14 (GeO_2) : 0.25 ($SDA(OH)_2$) : 5 (H_2O). Typically, a certain amount of germanium oxide (GeO_2) was dissolved in a solution of $SDA(OH)_2$ (1.0 mol L^{-1}). Then, TEOS was added and the mixture was gently stirred at room temperature until complete evaporation of the alcohol occurred. The resulting fluid gel was charged into a 25 ml Teflon-lined autoclave and heated at 175 °C for 20 days under agitation (~60 rpm). The solid product was separated by filtration, washed with distilled water and dried overnight at 65 °C. Occluded hexamethonium was removed from the samples by heating the products from room temperature to 300 °C at a rate of 1 °C min^{-1}, and this temperature was maintained for 3 h. The next step involved increasing the temperature at a rate of 1 °C min^{-1} up to 580 °C; this temperature was maintained under air flow (200 mL min^{-1}) for 3 h to remove the remaining organic residues.

Ge-rich zeolites *ITH-1* and *ITH-2* were prepared according to ref. 16. *N*,*N*,*N*′,*N*′-Tetramethyl-1,6-hexanediamine (TMHDA) was used as the structure directing agent. The synthesized suspension had a composition of (1–x) SiO_2 : x GeO_2 : 7 TMHDA : 1.4 HF : 44 H_2O, where x = 0.5 for *ITH-1* and x = 0.33 for *ITH-2*. The reaction mixture was heated at 175 °C for 6 days under static conditions.

The as-synthesized samples *ITH-1* and *ITH-2* were washed with distilled water, dried at 65 °C for 12 h and calcined at 650 °C for 8 h with a temperature ramp of 1 °C min^{-1} under air flow (200 mL min^{-1}).

2.4 Post-synthesis treatment

Post-synthesis alumination of **ITH** zeolites was performed by:

- stirring of the parent **ITH** zeolite in a 1 mol L^{-1} solution of $Al(NO_3)_3$ (1 g of zeolite per 100 ml of solution) at T = 80 °C and pH = 2.0 for 96 h.
- treatment of the parent **ITH** zeolite in a 1 mol L^{-1} solution of $Al(NO_3)_3$ (1 g of zeolite per 100 ml of solution) at T = 175 °C and pH = 2.0 for 24 h in an autoclave.

The solid product was centrifuged, extensively washed with distilled water until the filtrate became neutral and then dried overnight at room temperature.

The prepared samples are designated in the following way: *ITH-n/Al/temperature (°C)*.

2.5 Characterization

The crystallinity of all samples under investigation was determined by X-ray powder diffraction (XRD) using a Bruker AXS-D8 Advance diffractometer with a graphite monochromator, a position sensitive detector (Våntec-1) and CuKα radiation in Bragg–Brentano geometry at a scan rate of 0.25° (2θ) min^{-1}.

Nitrogen adsorption/desorption isotherms were measured using an ASAP 2020 (Micromeritics) static volumetric apparatus at liquid nitrogen temperature (−196 °C). Prior to sorption measurements, all samples were degassed with a turbomolecular pump at 300 °C for 8 h.

The size and shape of zeolite crystals were examined by scanning electron microscopy (SEM, JEOL JSM-5500LV microscope). For the measurement, the crystals were coated with a thin layer of platinum (~10 nm) in a BAL-TEC SCD-050 instrument.

The concentration of Al, Ge and Si in the zeolites was determined by energy dispersive X-ray spectroscopy (EDX) using a Jeol JSM 5600 instrument.

Solid-state ^{27}Al NMR spectra were obtained using a Bruker Advance III spectrometer equipped with a 9.4 T wide-bore superconducting magnet (^{1}H Larmor frequency of 400.13 MHz). The samples were packed into a conventional 4 mm zirconia rotor, and rotated at a MAS rate of 12.5 kHz using a Bruker 4 mm HFXY probe. A pulse of 1.5 μs ($\nu_1 \approx 100$ kHz) was applied. Signal averaging was carried out for 200 transients with a repeat interval of 2 s. The spectra were referenced to 1.1 M $Al(NO_3)_3$ in D_2O using solid $Al(acac)_3$ (δ_{iso} = 0 ppm, centre of gravity = −4.2 ppm at 9.4 T) as a secondary reference.

The concentration of Lewis (c_L) and Brønsted (c_B) acid sites was determined after adsorption of pyridine (Py) by FTIR spectroscopy using a Nicolet Protégé 460 Magna with a transmission MCT/A detector. The zeolites were pressed into self-supporting wafers with a density of 8.0–12 mg cm^{-2} and activated *in situ* at T = 450 °C and $p = 5 \times 10^{-5}$ Torr for 4 h. Pyridine adsorption was carried out at 150 °C and a partial pressure of 3.5 Torr for 20 min, followed by desorption for 20 min at the same temperature. Before adsorption, pyridine was degassed by freeze–pump–thaw cycles. All spectra were recorded with a resolution of 4 cm^{-1} by collecting 128 scans for a single spectrum at room temperature. The spectra were recalculated using a wafer density of 10 mg cm^{-2}. c_L and c_B were evaluated from the integral intensities of bands at 1454 cm^{-1} (c_L) and 1545 cm^{-1} (c_B) using extinction coefficients, ε(L) = 2.22 cm μmol^{-1} and ε(B) = 1.67 cm μmol^{-1}.[20]

A relatively large probe molecule 2,6-di-*tert*-butylpyridine (DTBP) was used to determine the accessibility of acid sites in the prepared zeolites.[21] The adsorption of DTBP took place at 150 °C for 15 min at an equilibrium vapour pressure of the probe molecule. Desorption proceeded at the same temperature for 1 h followed by collection of spectra at room temperature. The extinction coefficients determined in ref. 20 were used for the evaluation of c_B adsorbing DTBP.

2.6 Tetrahydropyranylation of alcohols

The catalytic experiments were performed in the liquid phase under atmospheric pressure at room temperature (25 °C) in a multi-experiment workstation StarFish (Radleys Discovery Technologies). Before use, the catalyst (100 mg) was activated at 450 °C for 90 min at a rate of 10 °C min^{-1}. Typically, alcohol (*i.e.* methanol, 1-propanol or 1-hexanol, 9 mmol), mesitylene (0.4 g, internal standard), hexane (10 ml, solvent) and the catalyst (100 mg) were placed in a two-necked vessel equipped with a thermometer. DHP (15 mmol) was then added into the vessel. Samples of the reaction mixture were taken periodically and analyzed by using an Agilent 6850 GC equipped with a nonpolar DB-5 column (length 20 m, diameter 0.180 mm, and film thickness 0.18 mm) and a flame ionization detector.

The reaction products were identified by using a Thermo Finnigan Focus DSQ II single quadrupole GC/MS.

3. Results and discussion

The X-ray diffraction patterns of germanosilicate **ITH** zeolites (Fig. 1) used as starting materials for alumination match well with those reported in the literature.[22] In contrast to *ITH-1* and *ITH-2* possessing platelet-like crystals, *ITH-6* is characterized by needle-like crystals (Fig. 2). While samples *ITH-1* and *ITH-2* present separated crystals of remarkably higher size (Fig. 2A and D, Table 1), the Ge-poor *ITH-6* sample shows agglomerates of tiny crystals (Fig. 2G, Table 1). This result may be connected with a higher rate of crystal growth in the presence of TMHDA acting as a SDA for the *ITH-1* and *ITH-2* samples. The broader and less intense diffraction lines characteristic of the *ITH-6* zeolite, in comparison to those of the *ITH-1* and *ITH-2* samples (Fig. 1), are consistent with the smaller size of *ITH-6* crystals (Fig. 2). *ITH-1* and *ITH-2* zeolites exhibit type I isotherms (Fig. 3A, B) characteristic of microporous solids and are characterized by micropore volumes of 0.112 and 0.125 cm^3 g^{-1}, respectively (Table 3). *ITH-6* germanosilicate representing quite small crystals (*ca.* 5.0 × 0.5 × 0.5 μm) showed uptake in the range of p/p_s = 0.8–1.0 (Fig. 3C) most probably attributed to filling of the intercrystalline space.

Chemical analysis of the **ITH** zeolites agrees with the composition of the corresponding gels showing increasing Si/Ge ratio in the solids with decreasing Ge concentration in the reaction mixture (Table 1). However, while the chemical composition of the Ge-poor *ITH-6* zeolite (Si/Ge = 5.8) corresponds to Si/Ge in the initial gel, Ge-rich *ITH-1* (Si/Ge = 2.5) and *ITH-2* (Si/Ge = 4.4) samples are characterized by *ca.* twice as low Si/Ge ratios compared to those in the reaction mixture (Table 1). This agrees with the results obtained in ref. 15 and

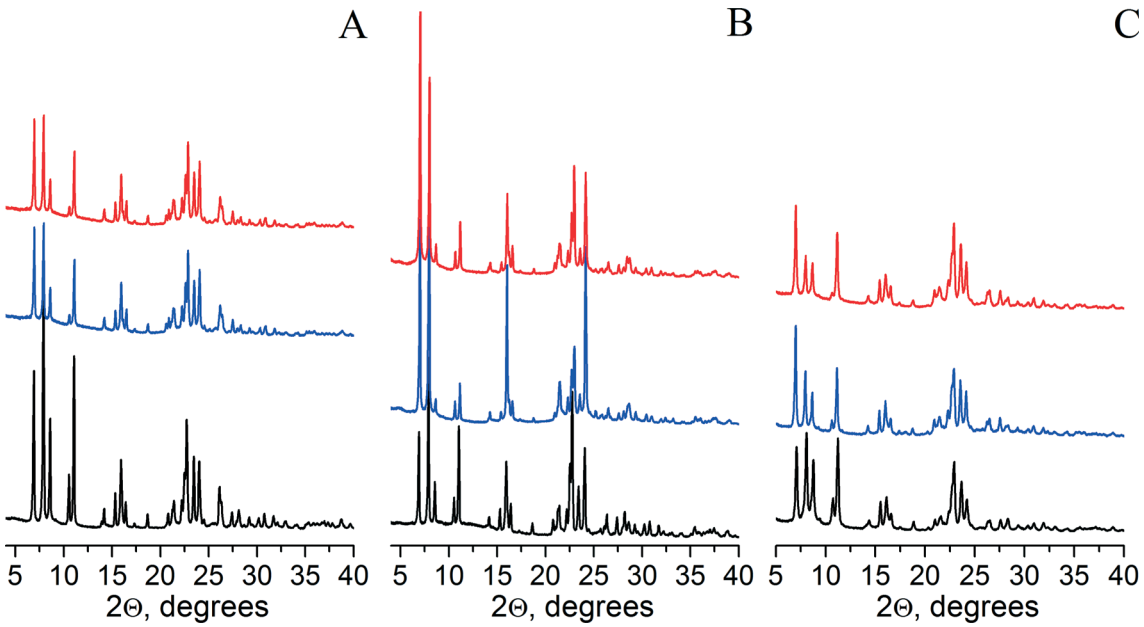

Fig. 1 XRD patterns of *ITH-1* (A), *ITH-2* (B), and *ITH-6* (C) zeolites: initial germanosilicates (black), *ITH-n/Al/80* (blue) and *ITH-n/Al/175* (red).

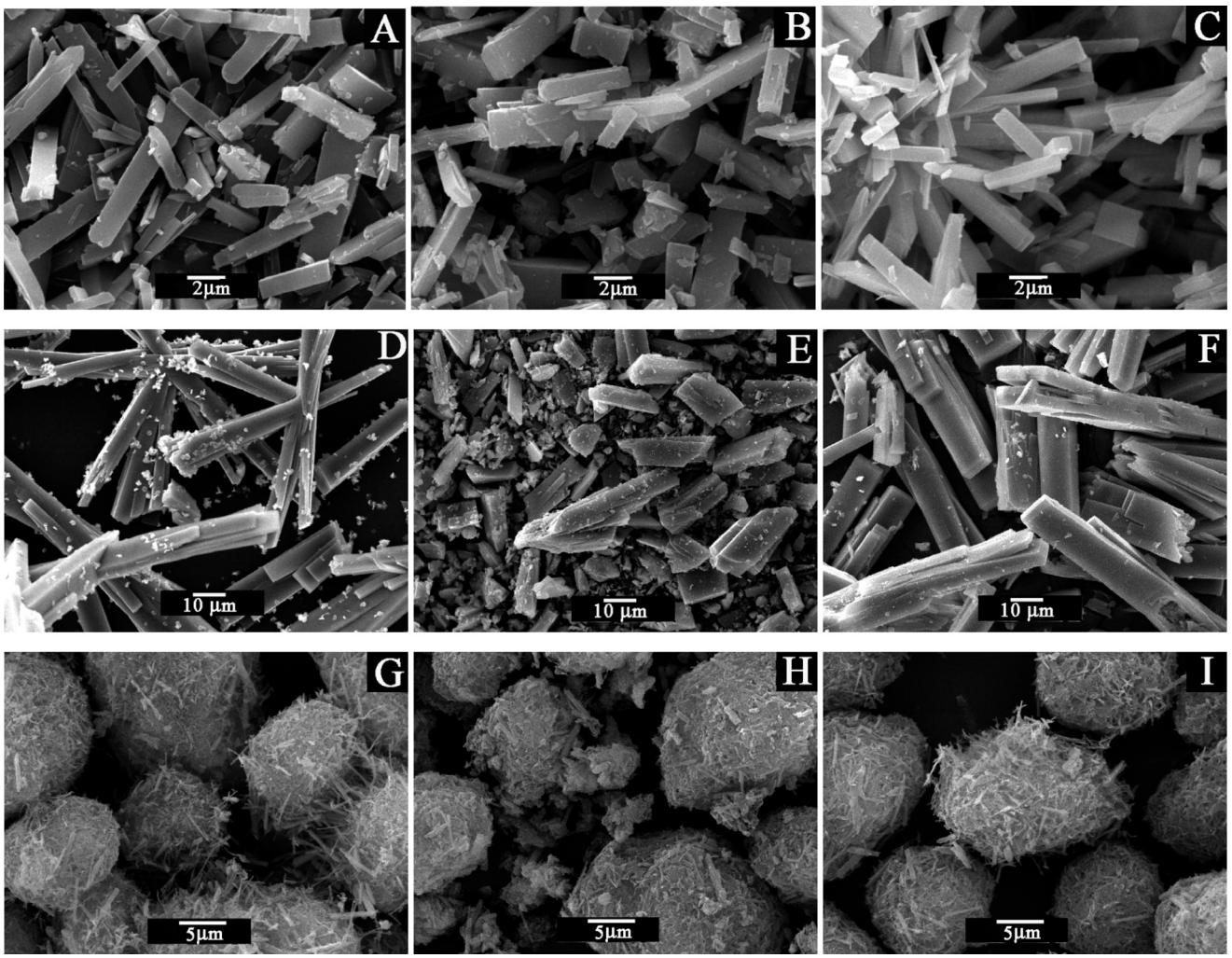

Fig. 2 SEM images of **ITH** zeolites under investigation: *ITH-1* (A); *ITH-1/Al/80* (B); *ITH-1/Al/175* (C); *ITH-2* (D); *ITH-2/Al/80* (E); *ITH-2/Al/175* (F); *ITH-6* (G); *ITH-6/Al/80* (H); *ITH-6/Al/175* (I).

Table 1 Chemical composition and textural characteristics of germanosilicate **ITH** zeolites under investigation

Sample	Chemical composition of zeolites, mol.%		Si/Ge		Crystal size, μm
	Si	Ge	Reaction mixture	Zeolite	
ITH-1	71.4	28.6	1	2.5	10.0 × 2.5 × 1.0
ITH-2	81.5	18.5	2	4.4	40.0 × 5.0 × 5.0
ITH-6	85.6	14.5	6	5.8	5.0 × 0.5 × 0.5

16 and may be related with "saturation" of T-sites in D4Rs and $[4^1 5^2 6^2]$ cages.

It should be noted that Ge preferentially occupies positions in D4Rs forming [4Si;4Ge] domains regularly located in-between silica layers in *ITH-1* and *ITH-2*, while both pure silica [8Si] and Si-rich D4Rs [7Si;1Ge] were detected in Ge-poor (Si/Ge > 5) **ITH** zeolites.[23]

3.1 The structure and textural properties of post-synthetically treated ITH zeolites

As it was shown in ref. 23, acidic treatment of **ITH** zeolites having appropriate amounts of Ge in D4R SBUs (*i.e.* $Si/Ge_{D4R} \leq 1$, like in the *ITH-1* sample) results in zeolite disassembly, *e.g.* the formation of layered materials possessing the same topology of the layers as the initial **ITH** zeolite. In contrast, all **ITH** zeolites subjected to alumination in acidic medium (pH = 2.0) at T = 80 °C or 175 °C still display sharp diffraction lines at the characteristic 2-theta positions, which proves the preservation of the structure ordering of the samples (Fig. 1). This indicates that Al acts as a "stabilizer" preventing the disassembly of the Ge-rich **ITH** zeolite (*i.e. ITH-1*) in acidic medium. The mentioned effect was also observed for the **IWR** zeolite in ref. 17 and may be connected with rapid healing of defects formed in the course of hydrolysis of Ge–O–Si bonds with Al. No diffraction lines of $Al(NO_3)_3$ or other crystalline admixtures were observed in the XRD patterns of **ITH** zeolites after employing the alumination procedures described in this study. The decrease in the intensity of diffraction lines of **ITH** zeolites subjected to alumination, which is especially pronounced in the Ge-rich *ITH-1* sample (Fig. 1A), likely originates from diminishing of the framework density caused by leaching of the framework Ge atoms under the conditions used (Table 2). The aluminated samples showed drastically higher Si/Ge ratios (12.6–158) compared with parent **ITH** zeolites (Si/Ge = 2.5–5.8). The magnitude of Ge extraction depends on both the temperature of treatment and the size of zeolite crystals. While *ITH-2/Al/80* and *ITH-2/Al/175* characterized by the bulkiest crystals (40.0 × 5.0 × 5.0 μm, Table 1) show close Si/Ge ratios (Table 2), a higher drop in Ge concentration at 175 *vs.* 80 °C was observed for *ITH-1* (10.0 × 2.5 × 1.0 μm) and especially *ITH-6* zeolites (5.0 × 0.5 × 0.5 μm). This result indicates the role of diffusion in the degermanation process and is in agreement with previous observations on the influence of zeolite crystal size on the dealumination[24] and desilication[25] outcome.

While the results of chemical analysis indicate increasing concentration of Al (Table 2), the solid-state ^{27}Al MAS NMR spectra of all aluminated samples (Fig. 3) show the presence of both tetrahedral AlO_4 (shift ranges of 50–80 ppm) and octahedral AlO_6 species (−10–15 ppm).[26] The Ge-rich *ITH-1* and *ITH-2* zeolites aluminated at 80 or 175 °C and *ITH-6/Al/175* sample show a dominant peak at −54 ppm (~90% of the integrated signal intensity) evidencing the incorporation of most aluminium atoms into the framework of the zeolites (Fig. 3). In contrast, *ITH-6/Al/80* shows a dominant reflex at 0 ppm (76% of the integrated intensity, Table 2) attributed to AlO_6 species. It seems that the output of alumination is

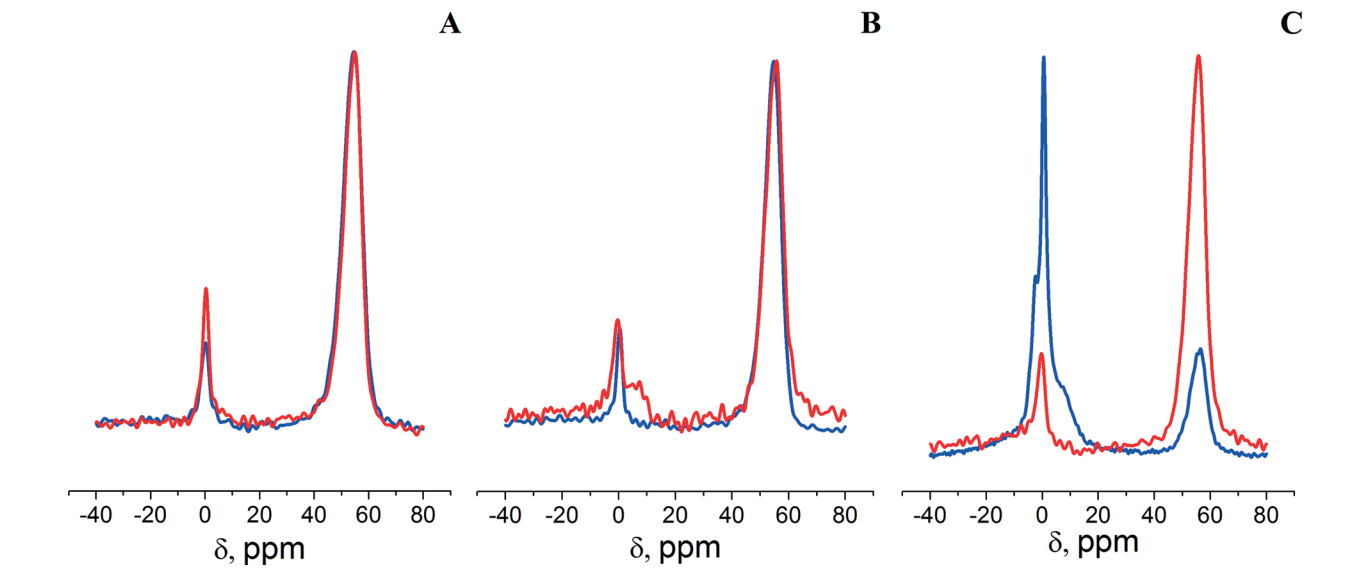

Fig. 3 ^{27}Al MAS NMR spectra of *ITH-1* (A), *ITH-2* (B), and *ITH-6* (C) zeolites: *ITH-n/Al/80* (blue) and *ITH-n/Al/175* (red).

Table 2 Chemical composition of ITH zeolites subjected to alumination

Sample	Chemical composition, mol.% Al	Ge	Si	Si/Ge	Al_{Th}[a], mol.%
ITH-1	—	28.6	71.4	2.5	—
ITH-1/Al/80	2.6	6.8	90.6	13.3	92
ITH-1/Al/175	4.3	2.2	93.5	42.5	88
ITH-2	—	18.5	81.5	4.4	—
ITH-2/Al/80	1.5	7.0	91.5	13.0	91
ITH-2/Al/175	2.1	7.2	90.7	12.6	84
ITH-6	—	14.5	85.6	5.8	—
ITH-6/Al/80	6.7	4.3	89.0	21.0	24
ITH-6/Al/175	4.0	0.6	95.0	158	89

[a] Calculated based on the integral intensities of peaks at 0 and 60 ppm in the ^{27}Al NMR spectra.

dependent on the rates of 3 processes, *i.e.* 1) extraction of Ge leading to the formation of silanol defects (*vide infra*), 2) healing of formed defects with Al leading to the formation of Brønsted acid sites, and 3) precipitation of oxo-Al species in the internal/intercrystalline voids resulting in deposition of extra-framework species. The total amount of Al as well as the ratio between framework and extra-framework Al species (Table 2) depends on both the treatment conditions and intrinsic properties of the initial germanosilicate (*i.e.* crystal size, Si/Ge ratio). Increasing the temperature of treatment results in an increase in the concentration of Al that is incorporated into the framework of *ITH-1* and *ITH-6* zeolites. In contrast, the concentration of Al in *ITH-2* zeolites possessing the bulkiest crystals does not depend significantly on the temperature of treatment. This result is likely connected with either diffusional restrictions for Ge extraction or Al penetration into bulky crystals. On the other hand, the contamination of extra-framework Al species is favourable for *ITH-6* zeolites possessing tiny crystals when aluminated at 80 °C (Table 2).

The shape of **ITH** platelet-like crystals remained intact during alumination (Fig. 2), while *ITH-1/Al/80* (Fig. 2B) and *ITH-2/Al/80* (Fig. 2E) showed an increased fraction of cracked tiny crystals (1–3 μm) in comparison with the parent *ITH-1* (Fig. 2A) and *ITH-2* (Fig. 2D) zeolites. In contrast, *ITH-1/Al/175* (Fig. 2C) and *ITH-2/Al/175* (Fig. 2F) zeolites treated under hydrothermal conditions showed crystals of uniform size close to that of the parent germanosilicates. This result is probably connected with acceleration of the dissolution/precipitation processes at elevated temperature *via* Ostwald ripening of **ITH** crystals under hydrothermal conditions. It seems that alumination at higher temperature resulted in accelerated and more complete recrystallization of *ITH-n* zeolites, while low temperature treatment led to deterioration of the crystal morphology (destruction or conglutination, Fig. 2).

The nitrogen isotherms provide valuable information on the textural properties of aluminated **ITH** zeolites when compared with the parent ones. In contrast to parent germanosilicate *ITH-1* and *ITH-2* zeolites (Fig. 4A, B) exhibiting type I isotherms, zeolites *ITH-1/Al/80* and *ITH-2/Al/80* aluminated at 80 °C show isotherms of type I with a hysteresis loop of H4 characteristic of microporous solids with a broad pore size distribution. The increase in the average pore size of *ITH-1* and *ITH-2* zeolites treated with $Al(NO_3)_3$ solution in acidic medium is most probably connected with breaking of hydrolytically unstable Ge–O(Si) bonds resulting in the increasing void volume. A similar process of mesopore formation in the course of the treatment of germanosilicate **IWW** zeolites with hydrochloric acid at elevated temperature was also observed in ref. 27. The increase in the alumination temperature leads to an increased fraction of mesopores in

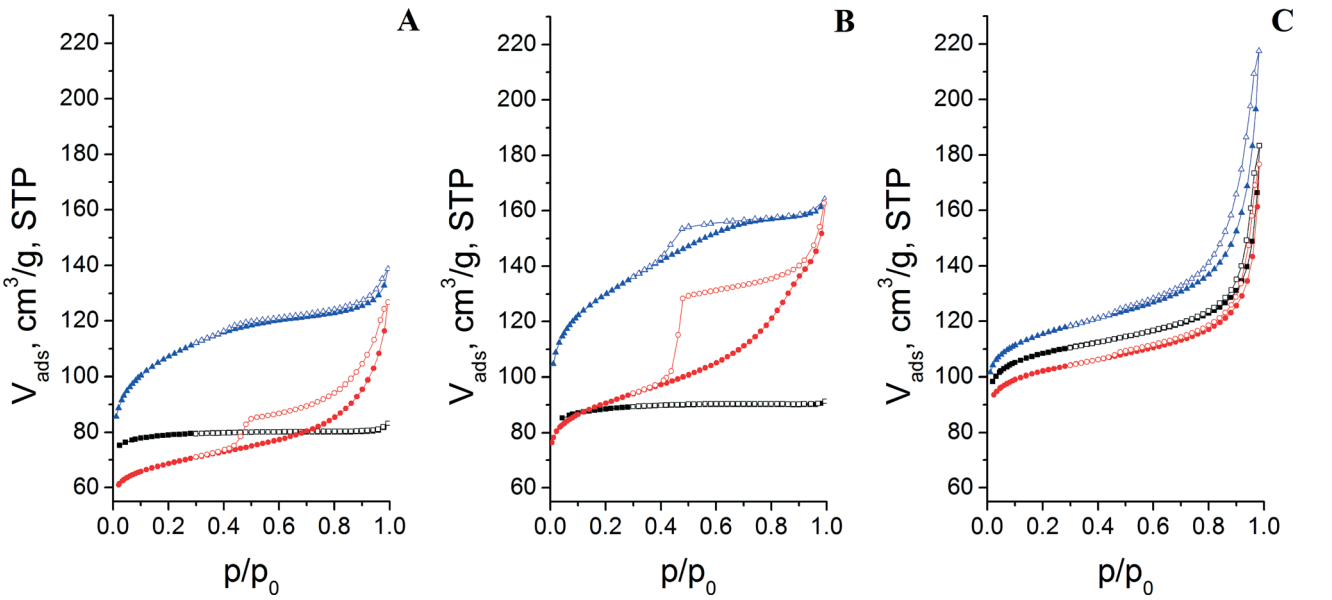

Fig. 4 Nitrogen adsorption (●) and desorption (○) isotherms of *ITH-1* (A), *ITH-2* (B), and *ITH-6* (C) zeolites: initial germanosilicates (black), *ITH-n/Al/80* (blue) and *ITH-n/Al/175* (red).

Table 3 Textural characteristics of ITH zeolites subjected to alumination

Sample	V_{micro}[a], $cm^3\ g^{-1}$	V_{meso}[b], $cm^3\ g^{-1}$	S_{BET}[c], $m^2\ g^{-1}$	S_{ext}[a], $m^2\ g^{-1}$
ITH-1	0.112	0.007	285	23
ITH-1/Al/80	0.103	0.05	330	143
ITH-1/Al/175	0.080	0.12	207	62
ITH-2	0.125	0.005	313	28
ITH-2/Al/80	0.124	0.07	400	166
ITH-2/Al/175	0.101	0.17	275	90
ITH-6	0.138	0.13	321	68
ITH-6/Al/80	0.141	0.18	345	86
ITH-6/Al/175	0.130	0.13	303	64

[a] The micropore volume and external surface area were evaluated using the *t*-plot method. [b] Evaluated using the BJH method. [c] The surface area was evaluated using adsorption branch in the range p/p_s = 0.05–0.25.

ITH-1/Al/175 and *ITH-2/Al/175* both exhibiting combined type I and type IV isotherms typical of hierarchical micro/mesoporous materials. It should be noted that a contribution of Si extraction in the formation of mesopores at 175 °C cannot be excluded, since *ITH-2/Al/80* and *ITH-2/Al/175* characterized by close Si/Ge ratios (Table 2) showed drastically different nitrogen adsorption/desorption isotherms (Fig. 4). In contrast, alumination does not significantly impact the pore system of the Ge-poor *ITH-6* zeolite. Both aluminated *ITH-6/Al/80* and *ITH-6/Al/175* zeolites or the parent *ITH-6* germanosilicate possessed similar adsorption/desorption isotherms of type I showing interparticle adsorption in the range of p/p_0 = 0.8–1.0 (Fig. 4C). The formation of extra porosity not observed during alumination of the Ge-poor *ITH-6* zeolite with $Al(NO_3)_3$ solution is likely caused by "unsuitable" distribution of extractable Ge atoms in the framework (the absence of [4Si;4Ge] domains according to the NMR data[2,3]).

Both *ITH-6* zeolite and its aluminated derivatives *ITH-6/Al/80* and *ITH-6/Al/175* are characterized by high V_{meso} values, which is related to adsorption of nitrogen in the interparticle space of the crystals (Table 3). Alumination of *ITH-1* and *ITH-2* zeolites decreased the micropore volume but increased the volume of mesopores in the range of 0.3–0.8 of p/p_0 (Table 3). Increased mesopore volume corresponds to the formation of extra pores in the course of Ge extraction during alumination of *ITH-1* and *ITH-2* enhancing with increasing temperature of the treatment. The higher values of external surface area S_{ext} for *ITH-1/Al/80* and *ITH-2/Al/80* with respect to the initial germanosilicates (Table 3) agree with the results of SEM showing the decreasing average crystal size after alumination of Ge-rich **ITH** zeolites at 80 °C (Fig. 2).

3.2 The nature and concentration of acid sites

FTIR spectroscopy was carried out to investigate the evolution of OH groups during alumination of **ITH** zeolites with different chemical compositions; the relevant spectra are depicted in Fig. 5A. The parent germanosilicates showed two absorption bands (at *ca.* 3745 and 3633–3653 cm^{-1}) in the region of 3800–3500 cm^{-1}. While the intensity of the band at 3745 cm^{-1} attributed to silanol groups increased with decreasing crystal size of germanosilicate **ITH** zeolites (*ITH-2* < *ITH-1* < *ITH-6* (Fig. 5A, Table 1)), a broad absorption band at 3633–3653 cm^{-1} attributed to external Ge–OH groups[28] grew with increasing Ge content in the following sequence: *ITH-6* < *ITH-2* < *ITH-1*.

The increased absorption band at 3745 cm^{-1} in the spectra of the *ITH-n/Al/80* zeolite with respect to the parent germanosilicate indicates formation of silanol defects under the conditions used (Fig. 5A). In contrast, *ITH-n/Al/175* and *ITH-n* zeolites showed absorption bands at 3745 cm^{-1} of comparable intensities (Fig. 5A). This indicates acceleration of Al incorporation into the framework of **ITH** zeolites accompanied with some healing of silanol defects with increasing temperature of treatment. In agreement with this assumption, the **ITH** zeolites aluminated at 175 °C are characterized by more intensive absorption bands assigned to bridging hydroxyl groups (*ca.* 3620 cm^{-1}, Fig. 5A) compared with the samples treated at 80 °C.

The incorporation of Al atoms into the framework of **ITH** zeolites in the course of post-synthesis treatment was confirmed by FTIR spectroscopy of adsorbed pyridine. The appearance of the absorption band at 1545 cm^{-1} assigned to the pyridinium ion in the spectra of the aluminated **ITH** zeolites clearly evidences the incorporation of aluminium into the framework positions (Fig. 5B). In addition, alumination caused the increase in the intensity of the absorption band at 1455 cm^{-1}, which is obviously connected with the increased concentration of Lewis acid centres [25] in the aluminated **ITH** zeolites in comparison with the initial germanosilicates.

The concentrations of Brønsted and Lewis acid sites determined from the integral intensities of the bands at 1545 and 1455 cm^{-1} using extinction coefficients[20] are given in Table 4. The *ITH-6/Al/80* (c_B = 97, c_L = 194 μmol g^{-1}) and *ITH-6/Al/175* (c_B = 239, c_L = 150 μmol g^{-1}) samples having the smallest crystals showed the highest concentrations of incorporated acid centres despite a relatively low concentration of hydrolytically unstable Ge–O(Si) bonds (Table 1). For zeolites of comparable crystal size (*e.g. ITH-1*, *ITH-2*), the amount of incorporated acid centres increased with decreasing Si/Ge ratio in the parent germanosilicates.

This may be connected with 1) increasing concentration of hydrolytically unstable Ge–O(Si) bonds being the source of defects in the second step, condensing with aluminium ions to form acid centres and 2) increasing average size of pores developed in the course of hydrolysis of available Ge–O(Si) bonds facilitating diffusion of aluminium ions to the formed defects. In this way, alumination of the *ITH-1* zeolite containing 28.6 mol.% Ge (Table 1) generated a higher amount of acid centres (200 and 240 μmol g^{-1}, Table 4), compared with *ITH-2* (18.9 mol.% Ge)-derived samples (157 and 175 μmol g^{-1}, Table 4). A remarkably increased concentration of formed Brønsted acid centres (1.5–2.5 times) and a slightly decreased amount of Lewis acid sites (Table 3) with increasing temperature of alumination of **ITH** zeolites from 80 to 175 °C should be noticed.

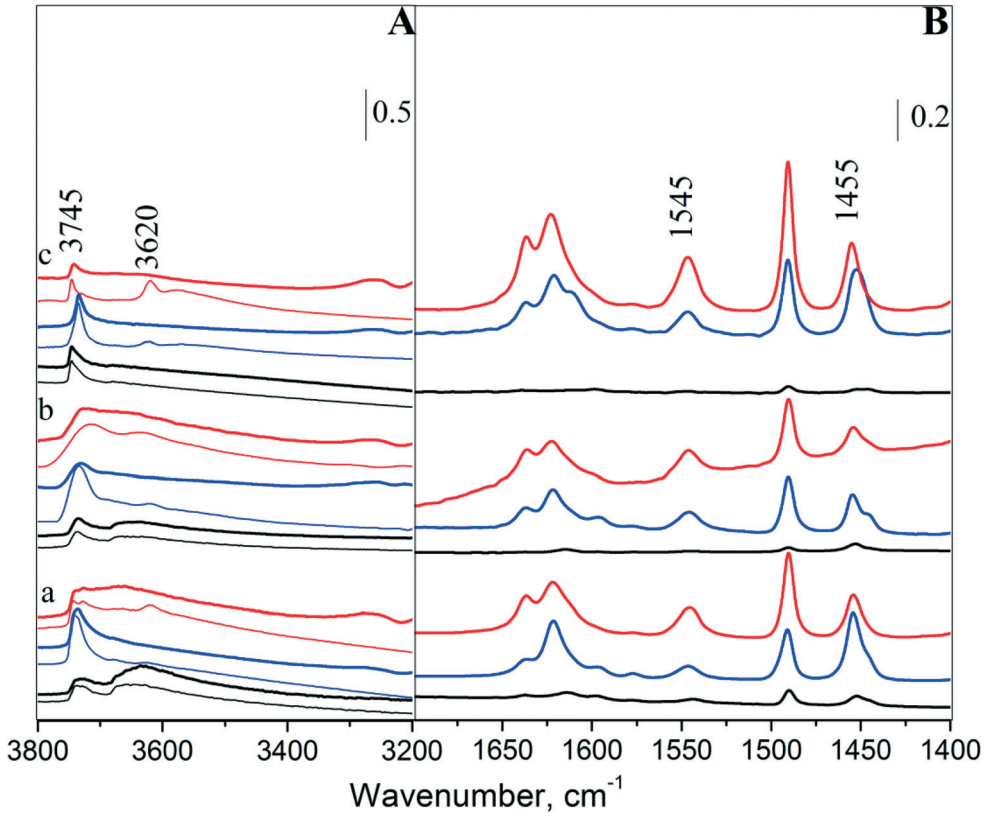

Fig. 5 IR spectra of *ITH-1* (a), *ITH-2* (b), and *ITH-6* (c) zeolites (initial germanosilicates (black), *ITH-n/Al/80* (blue) and *ITH-n/Al/175* (red)): (A) region of hydroxyl vibrations; (B) region of pyridine vibrations. Bottom/thin lines show spectra before adsorption of pyridine, while top/bold lines show spectra after adsorption of a base molecule.

At first sight, successful incorporation of Al atoms into the framework of medium-pore **ITH** zeolites in the course of post-synthesis treatment seems to contradict the literature results,[29,30] thoroughly disproving aluminium incorporation into medium-pore boralites in acidic medium with the inner void being inaccessible to bulky hydrated aluminium cations. However, these studies focused only on (boro)silicate zeolites. The presence of hydrolytically unstable "domains" (*i.e.* D4R SBUs) in *ITH-1* and *ITH-2* zeolites seems to create the important prerequisites for the incorporation of Al atoms. Since the conditions for treatment (pH = 2.0, T = 80 or 175 °C) are sufficient for extraction of most Ge atoms from the framework (Table 2), it is reasonable to assume that the first stage of the overall process is the breaking of Si–O–Ge bonds in D4Rs.[23] This leads to the formation of silanol defects in all **ITH** zeolites under investigation (Fig. 5A) as well as the creation of ultramicro- and meso-pores in *ITH-1* or *ITH-2* zeolites (Fig. 4). Thus, the development of extra porosity in the course of *ITH-1* and *ITH-2* alumination seems to facilitate the penetration of hydrated aluminium cations into the inner volume of zeolite crystals followed by their condensation with Si–OH groups. At the same time, the "unsuitable" distribution of extractable Ge atoms in the framework (the absence of [4Si;4Ge] domains according to the NMR data[23]) of the *ITH-6* zeolite seems to prevent the formation of extra pores (Fig. 4C). For the latter sample, 75% of Al forms intercrystalline extra-framework species with octahedrally coordinated aluminium (Fig. 3), whereas the formation of Brønsted acid sites (Table 4) likely proceeds mainly on the outer surface of the crystals.

Noticeably, the concentration of framework Al (Al_{FR}, Table 4) calculated based on the results of ^{27}Al NMR spectroscopy exceeds the total concentration of acid sites determined using Py as the probe molecule. This is obviously

Table 4 The concentration of Lewis and Brønsted acid sites within **ITH** zeolites determined by means of FTIR spectroscopy of adsorbed Py and DTBP

Sample	c_B, μmol g^{-1}		c_L, μmol g^{-1}	$c_{\sum}$, μmol g^{-1}	Al_{FR}[a], μmol g^{-1}	$c_{\sum}/Al_{FR}$, %
	Pyridine	DTBP	Pyridine			
ITH-1	—	—	26	26	—	—
ITH-1/Al/80	60	24	140	200	381	53
ITH-1/Al/175	140	4	100	240	624	38
ITH-2	—	—	20	20	—	—
ITH-2/Al/80	90	21	67	157	216	72
ITH-2/Al/175	127	1	48	175	279	62
ITH-6	—	—	13	13	—	—
ITH-6/Al/80	97	10	194	291	371	78
ITH-6/Al/175	239	8	150	389	594	65

[a] Calculated based on the results of chemical analysis and relative integral intensity of the peak at 60 ppm in the ^{27}Al NMR spectra.

connected with different accessibilities of the incorporated Al atoms being dependent on the treatment conditions and crystal size of the aluminated **ITH** zeolites. A lower fraction of acid centres detectable with Py is characteristic of *ITH-n/Al/175* (38–65%, Table 4) *vs. ITH-n/Al/80* zeolites (53–78%, Table 4). This result may indicate the incorporation of a higher amount of Al into the "inner" domains of **ITH** crystals with increasing temperature of alumination. Remarkably higher concentrations of surface Brønsted acid centres for *ITH-1/Al/80* to *ITH-1/Al/175* and similarly for *ITH-2*-derived samples (Table 4) were also detected using FTIR spectroscopy of adsorbed DTBP (the size of the DTBP molecule is about 7.9 Å,[21] which is higher than the diameter of 10-ring channels in zeolites). The higher accessibility of acid centres in *ITH-2*-derived samples (62 and 72%, Table 4) *vs. ITH-1* derivatives (38 and 53%, Table 4) is probably connected with the larger fraction of mesopores within *ITH-2/Al vs. ITH-1/Al* (Table 3). Naturally, *ITH-6/Al* zeolites characterized by tiny crystals (Fig. 2) showed the highest accessibility of acid centres (65 and 78%, Table 4) among the zeolites under investigation. According to the results of FTIR spectroscopy of adsorbed DTBP, *ITH-6* zeolites aluminated at different temperatures insignificantly differ in the concentration of surface Brønsted acid sites detected with DTBP (8–10 μmol g^{-1}, Table 4).

3.3 Catalytic performance of Al-substituted ITH zeolites in tetrahydropyranylation of alcohols

The activity of various heterogeneous catalysts in the tetrahydropyranylation of alcohols may be attributed to both Brønsted and Lewis acid sites.[18,31] The catalytic behavior of aluminated **ITH** zeolites was investigated in the tetrahydropyranylation of methanol, 1-propanol and 1-hexanol.

While practically no conversion of substrates was observed over the initial germanosilicate **ITH** zeolites possessing only a small amount of weak Lewis acid centres (Fig. 6, Table 4), the only products of alcohol transformation formed in the reaction mixture over the Al-containing zeolites under investigation were targeted tetrahydropyranyl ethers (Scheme 1). The relative amount of dimers formed in competitive bimolecular dimerization of DHP did not exceed 6 mol.%.

The yield of tetrahydropyranyl ether obtained in the reaction of methanol and DHP after 1200 min was found to increase in the following order of catalysts: *ITH-2/Al/175* (25%) < *ITH-1/Al/175* (58%) < *ITH-1/Al/80* (85%) < *ITH-6/Al/80* (100%) = *ITH-6/Al/175* (100%) = *ITH-2/Al/80* (100%) (Fig. 6). Noticeably, *ITH-n/Al/80* (n = 1, 2) samples characterized by higher accessibility of acid sites performed better than *ITH-n/Al/175* (n = 1, 2) zeolites. In particular, *ITH-2/Al/175* possessing a higher concentration of acid centres than *ITH-2/Al/80* (175 *vs.* 157 μmol g^{-1}, Table 4) showed a remarkably lower initial rate in methanol tetrahydropyranylation (80×10^{-5} *vs.* 430×10^{-5} mmol h^{-1}, Fig. 7). At the same time, while *ITH-1/Al/80* (S_{ext} = 143 m^2 g^{-1}, Table 3) and *ITH-1/Al/175* (S_{ext} = 62 m^2 g^{-1}, Table 3) were characterized by similar initial reaction rates in methanol transformation (110–150 × 10^{-5} mmol h^{-1}, Fig. 7A). *ITH-1/Al/80* with a larger S_{ext} (accessibility of acid sites) showed a higher yield of the target ether (Fig. 7B). The obtained results may indicate that diffusion constraints exist in the prepared micro/mesoporous **ITH** zeolites possessing big crystals (*i.e. ITH-1* and *ITH-2* aluminated derivatives) even when methanol is used as a substrate.

Diffusion limitations do not seem to play the decisive role in tetrahydropyranylation of methanol over aluminated *ITH-6* zeolites having the smallest crystals of 5.0 × 0.5 × 0.5 μm size (Table 1, Fig. 2H, I). In this way, *ITH-6/Al/80* (S_{ext} = 86 m^2 g^{-1},

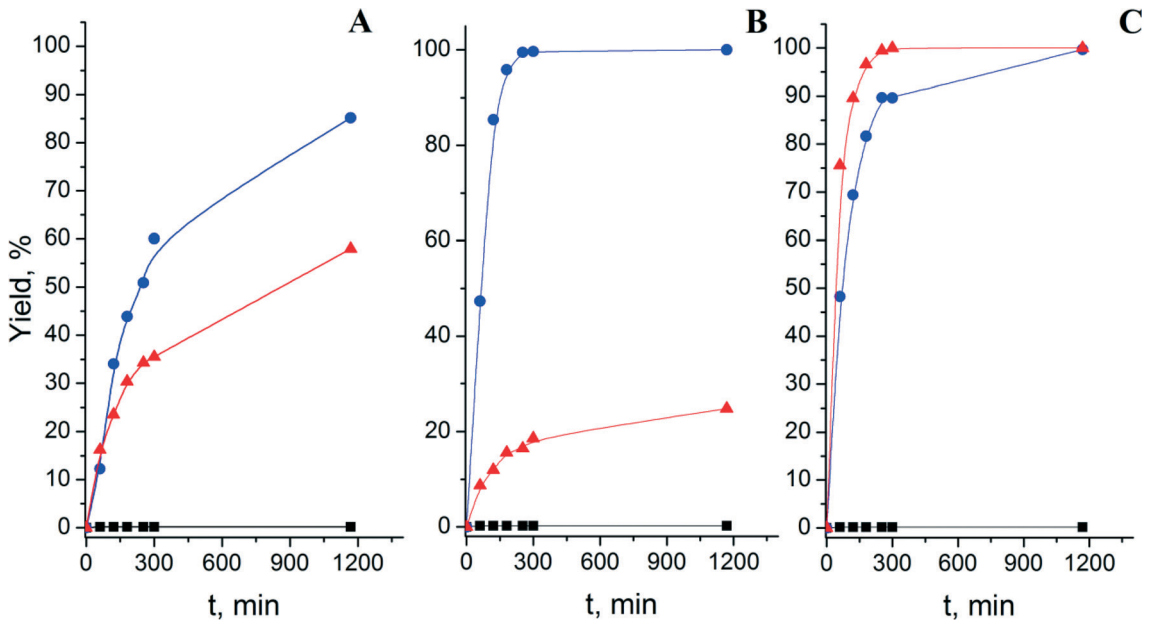

Fig. 6 Yield of tetrahydropyranyl ether *versus* time obtained in the reaction of methanol and DHP at 25 °C over *ITH-1* (A), *ITH-2* (B), and *ITH-6* (C)-derived zeolites: initial germanosilicates (black), *ITH-n/Al/80* (blue) and *ITH-n/Al/175* (red).

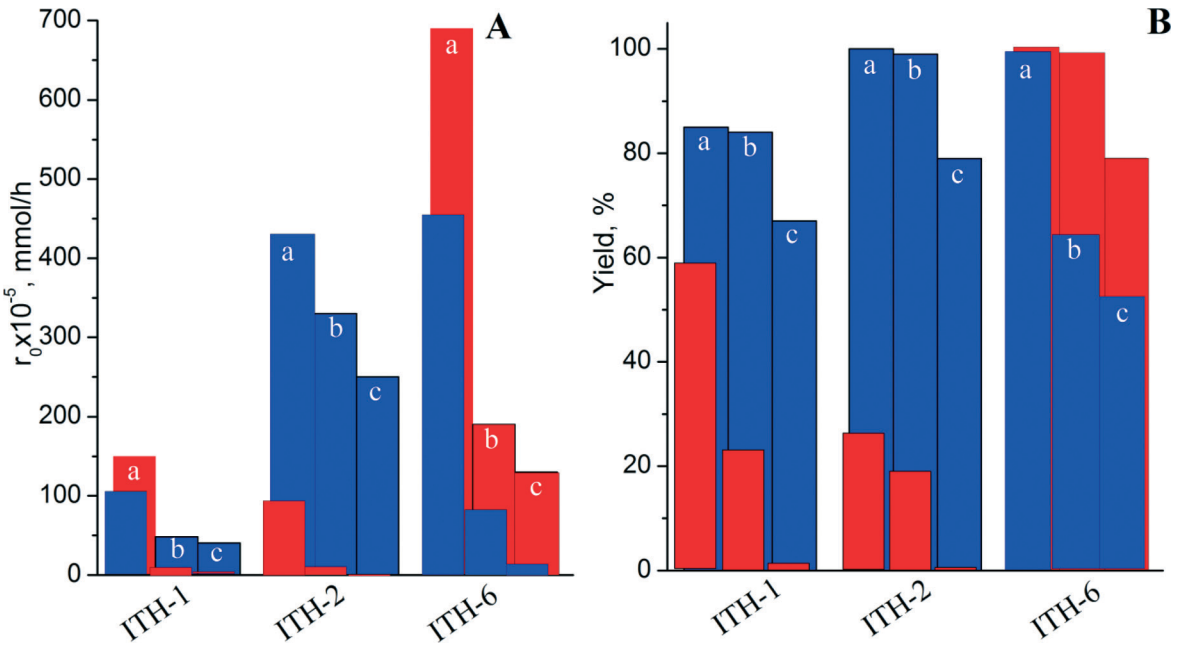

Fig. 7 Initial rate (A) and yield of tetrahydropyranyl ethers (B) formed in the reaction of methanol (a), 1-propanol (b) and 1-hexanol (c) over **ITH** zeolites aluminated at 80 °C ( ) and at 175 °C ( ).

Table 3) showed an initial rate 4 times higher in methanol tetrahydropyranylation (Fig. 7A) in comparison with *ITH-1/Al/80* (S_{ext} = 143 m^2 g^{-1}, Table 3) (Fig. 7A). The superior performance of *ITH-6/Al/80* having a higher total concentration of acid sites (291 *vs.* 200 μmol g^{-1}, Table 4) in transformation of methanol can be explained by taking into account the possibility of substrate activation by the "inner" acid centres. In contrast, *ITH-1/Al/80* (67–84% yield, Fig. 7B) performed better than *ITH-6/Al/80* (52–64% yield, Fig. 7B) when using bulkier 1-propanol and especially 1-hexanol as substrates. This result is likely connected with the increased concentration of external acid sites in *ITH-1/Al/80* possessing higher external surface area (143 m^2 g^{-1}, Table 3) *vs.* *ITH-6/Al/80* (86 m^2 g^{-1}, Table 3).

A decrease in the activity of all aluminated **ITH** samples (Fig. 7) was observed when the size of the reactants increased (methanol (kinetic diameter 3.6 Å) < 1-propanol (4.7 Å) < 1-hexanol (6.2 Å)).[32] Again, *ITH-1/Al/80* and *ITH-2/Al/80* showed higher initial rates of alcohol transformation (Fig. 7A) and yields of target ethers (Fig. 7B) *vs.* *ITH-1/Al/175* and *ITH-2/Al/175* possessing lower S_{ext} (accessibility of acid sites). It should be noted that the particular results of DTBP (a selective probe molecule for Brønsted sites[33]) adsorption and activity of the prepared *ITH-n/Al* samples in tetrahydropyranylation of alcohols can hardly be correlated without considering the total concentration of accessible acid sites (both Brønsted and Lewis) formed on the external surface. In particular, by comparing *ITH-1/Al/80* (S_{ext} = 143 m^2 g^{-1}, Table 3) and *ITH-2/Al/80* (S_{ext} = 166 m^2 g^{-1}, Table 3), a very similar amount of external Brønsted acid sites (Table 4) gives massively different activities (Fig. 7), which may be related to the higher S_{ext} of more active *ITH-2/Al/80.* On the other hand, the catalytic activity of the prepared Al-substituted **ITH** zeolites cannot be correlated only with their textural characteristics. For instance, *ITH-1/Al/175* (S_{ext} = 62 m^2 g^{-1}, Table 3) showed higher yields, despite having a lower S_{ext} than *ITH-2/Al/175* (S_{ext} = 90 m^2 g^{-1}, Table 3). This agrees with the higher concentration of surface Brønsted acid sites in *ITH-1/Al/175* (Table 4).

In contrast, the total acidity likely determines the catalytic behavior of *ITH-6* aluminated derivatives when 1-propanol and 1-hexanol are used as substrates. *ITH-6/Al/80* possessing a lower total number of acid sites ($c_{\sum}$ = 291 μmol g^{-1}) shows lower initial rates and yields in tetrahydropyranylation of 1-propanol and 1-hexanol than *ITH-6/Al/175* ($c_{\sum}$ = 389 μmol g^{-1}) (Fig. 7) despite having a similar number of external Brønsted acid sites (Table 4) and a higher S_{ext} (Table 3). This result can be rationalized through considering the lower pass length of reacting molecules into and off the tiny crystals of Al-containing *ITH-6* zeolites and assuming activation of substrate molecules (kinetic diameters <6.2 Å) with acid centres inaccessible to DTBP (kinetic diameter = 7.9 Å) within the *ITH-6/Al* catalysts.

The *ITH-2/Al/80* zeolite possessing the highest value of S_{ext} (166 m^2 g^{-1}, Table 3) showed the highest initial rates when 1-propanol ($r_0 = 330 \times 10^{-5}$ mmol h^{-1}) and 1-hexanol ($r_0 = 250 \times 10^{-5}$ mmol h^{-1}) were used as substrates (Fig. 7). However, it should be noted that the yields achieved over *ITH-2/Al/80* possessing relatively high S_{ext} and *ITH-6/Al/175* having the highest concentration of acid sites are comparable (Fig. 7). This agrees with the higher concentration of acid centres activating the substrate molecules at the initial time within ITH-2/Al/80 (*e.g.* surface acid centres), while involving the "inner" acid sites of *ITH-6/Al/175* in the catalytic process as it progresses.

4. Conclusions

Alumination of the Ge-rich medium-pore **ITH** zeolites (Si/Ge = 2.5 and 4.4) in acidic medium (pH = 2) was found to result not only in the formation of strong Brønsted and Lewis acid sites but also in the development of extra porosity, related to extraction of Ge from D4Rs SBUs regularly arranged in the initial germanosilicates. In contrast, no extra pores were formed in the course of alumination of the Ge-poor **ITH** zeolites (Si/Ge = 5.8).

The chemical composition and crystal size of the initial zeolites as well as the temperature of post-synthesis treatment were shown to determine the total concentration and accessibility of formed acid centres as well as the ratio between Brønsted and Lewis acid sites.

For Ge-rich **ITH** zeolites showing bulky crystals (*e.g.* 10.0 × 2.5 × 1.0 μm), the amount of incorporated acid centres increased with decreasing Si/Ge ratio in the parent germanosilicate, which is likely connected with: 1) increased concentration of hydrolytically unstable Ge–O(Si) bonds being the source of defects further condensed with aluminium ions to form acid centres and 2) increased average size of pores developed during hydrolysis of available Ge–O(Si) bonds, which facilitate diffusion of aluminium ions to the formed defects. Ge-poor **ITH** zeolites possessing the smallest crystals (*i.e.* 5.0 × 0.5 × 0.5 μm) showed the highest concentration of incorporated acid centres (291 and 389 μmol g^{-1} for the samples aluminated at 80 and 175 °C, respectively).

The formation of larger pores at 175 °C enhanced the diffusion of Al species as well as the acceleration of the rates of condensation reactions leading to the formation of Si–O–Al bonds. This led to a remarkable increase (1.5–2.5 times) in the concentration of formed Brønsted acid centres and a slightly decreased amount of Lewis acid sites in the aluminated **ITH** zeolites independent of the chemical composition of the parent germanosilicates.

In contrast to alumination at 80 °C, treatment of germanosilicate **ITH** zeolites at 175 °C was accompanied with a decreasing fraction of framework Al atoms detectable with base probe molecules (*i.e.* pyridine, 2,6-di-*tert*-butylpyridine), *i.e.* the increased concentration of the "inner" acid sites.

The activity of the prepared Al-substituted **ITH** zeolites possessing big crystals (*e.g.* 10.0 × 2.5 × 1.0 μm) was found to be not dependent on the total concentration of acid centres, indicating diffusion constraints existing in the prepared micro/mesoporous **ITH** zeolites even when methanol was used as a substrate in the tetrahydropyranylation reaction. In general, Ge-rich **ITH** zeolites (Si/Ge = 2.5 and 4.4) aluminated at 80 °C and having higher S_{ext} and concentration of accessible acid sites performed better in tetrahydropyranylation of alcohols than the samples aluminated at 175 °C. In contrast, the activity of aluminated derivatives of Ge-poor **ITH** zeolites (Si/Ge = 5.8) possessing tiny crystals (*i.e.* 5.0 × 0.5 × 0.5 μm) increased with increasing total concentration of acid centres. A decrease in the activity of all aluminated **ITH** samples was observed when the size of the reactants increased (methanol (kinetic diameter 3.6 Å) < 1-propanol (4.7 Å) < 1-hexanol (6.2 Å)).

Acknowledgements

The authors thank Dr. Daniel Dawson (University of St. Andrews) for providing the NMR data. M. S. thanks the Czech Science Foundation for support through the project 14-30898P. M. O. acknowledges the Czech Science Foundation for the project 13-17593P. R. E. M. thanks the EPSRC for funding (EP/K025112/1 and EP/L014475/1).

Notes and references

1 D. Kubicka, I. Kubickova and J. Čejka, *Catal. Rev.: Sci. Eng.*, 2013, **55**, 1–78.
2 S. M. Csicsery, in *Stud. Surf. Sci. Catal.*, ed. H. K. Beyer, H. G. Karge, I. Kiricsi and J. B. Nagy, 1995, vol. 94, pp. 1–12.
3 W. J. Roth, P. Nachtigall, R. E. Morris, P. S. Wheatley, V. R. Seymour, S. E. Ashbrook, P. Chlubna, L. Grajciar, M. Polozij, A. Zukal, O. Shvets and J. Čejka, *Nat. Chem.*, 2013, **5**, 628–633.
4 P. S. Wheatley, P. Chlubná-Eliášová, H. Greer, W. Zhou, V. R. Seymour, D. M. Dawson, S. E. Ashbrook, A. B. Pinar, L. B. McCusker, M. Opanasenko, J. Čejka and R. E. Morris, *Angew. Chem. Int. Ed.*, 2014, **53**, 13210–13214.
5 A. Corma, M. J. Diaz-Cabanas, J. L. Jorda, F. Rey, G. Sastre and K. G. Strohmaier, *J. Am. Chem. Soc.*, 2008, **130**, 16482–16483.
6 M. Kubů, S. Zones and J. Čejka, *Top. Catal.*, 2010, **53**, 1330–1339.
7 S. Smeets, D. Xie, L. B. McCusker, C. Baerlocher, S. I. Zones, J. A. Thompson, H. S. Lacheen and H.-M. Huang, *Chem. Mater.*, 2014, **26**, 3909–3913.
8 J. Čejka, A. Vondrová, B. Wichterlová, G. Vorbeck and R. Fricke, *Zeolites*, 1994, **14**, 147–153.
9 A. Corma, M. Puche, F. Rey, G. Sankar and S. J. Teat, *Angew. Chem., Int. Ed.*, 2003, **42**, 1156–1159.
10 T. Boix, M. Puche, M. A. Camblor and A. Corma, *Synthetic porous crystalline material ITQ-13 its synthesis and use*, US 6,471,941.
11 M. V. Shamzhy, O. V. Shvets, M. V. Opanasenko, P. S. Yaremov, L. G. Sarkisyan, P. Chlubna, A. Zukal, V. R. Marthala, M. Hartmann and J. Cejka, *J. Mater. Chem.*, 2012, **22**, 15793–15803.
12 O. V. Shvets, M. V. Shamzhy, P. S. Yaremov, Z. Musilova, D. Prochazkova and J. Čejka, *Chem. Mater.*, 2011, **23**, 2573–2585.
13 R. Castaneda, A. Corma, V. Fornes, J. Martinez-Triguero and S. Valencia, *J. Catal.*, 2006, **238**, 79–87.
14 J. S. Buchanan, J. M. Dakka, X. Feng and J. G. Santiesteban, *Aromatics conversion with ITQ-13*, US7081556 B2.
15 J. A. Vidal-Moya, T. Blasco, F. Rey, A. Corma and M. Puche, *Chem. Mater.*, 2003, **15**, 3961–3963.
16 X. Ren, J. Liu, Y. Li, J. Yu and R. Xu, *J. Porous Mater.*, 2013, **20**, 975–981.
17 M. Shamzhy and F. S. d. O. Ramos, *Catal. Today*, 2015, **243**, 76–84.
18 G. Sartori, R. Ballini, F. Bigi, G. Bosica, R. Maggi and P. Righi, *Chem. Rev.*, 2003, **104**, 199–250.

19 G. Sastre, A. Pulido, R. Castañeda and A. Corma, *J. Phys. Chem. B*, 2004, **108**, 8830–8835.
20 C. A. Emeis, *J. Catal.*, 1993, **141**, 347–354.
21 M. A. Camblor, A. Corma, H. García, V. Semmer-Herlédan and S. Valencia, *J. Catal.*, 1998, **177**, 267–272.
22 C. Baerlocher, L. B. McCusker and D. H. Olson, *Atlas of zeolite framework types*, Elsevier, Amsterdam, 2007.
23 M. Shamzhy, M. Opanasenko, Y. Tian, K. Konysheva, O. Shvets, R. E. Morris and J. Čejka, *Chem. Mater.*, 2014, **26**, 5789–5798.
24 R. Dutartre, L. C. de Ménorval, F. Di Renzo, D. McQueen, F. Fajula and P. Schulz, *Microporous Mater.*, 1996, **6**, 311–320.
25 J. C. Groen, L. A. A. Peffer, J. A. Moulijn and J. Pérez-Ramírez, in *Stud. Surf. Sci. Catal.*, ed. S. Abdelhamid and J. Mietek, Elsevier, 2005, vol. 156, pp. 401–408.
26 in *Multinuclear Solid-State NMR of Inorganic Materials*, ed. J. D. M. Kenneth and E. S. Mark, Pergamon, 2002, vol. 6, pp. 271–330.
27 L. Burel, N. Kasian and A. Tuel, *Angew. Chem. Int. Ed.*, 2014, **53**, 1360–1363.
28 M. Moliner, M. J. Díaz-Cabañas, V. Fornés, C. Martínez and A. Corma, *J. Catal.*, 2008, **254**, 101–109.
29 C. Y. Chen and S. I. Zones, *Method for heteroatom lattice substitution in large and extra-large pore borosilicate zeolites*, US 6,468,501.
30 C.-Y. Chen and S. I. Zones, in *Zeolites and Catalysis*, Wiley-VCH Verlag GmbH & Co. KGaA, 2010, pp. 155–170.
31 P. G. M. Wuts and T. W. Greene, in *Greene's Protective Groups in Organic Synthesis*, John Wiley & Sons, Inc., 2006, pp. 431–532.
32 H. Wu, Q. Gong, D. H. Olson and J. Li, *Chem. Rev.*, 2012, **112**, 836–868.
33 K. Góra-Marek, K. Tarach and M. Choi, *J. Phys. Chem. C*, 2014, **118**, 12266–12274.

